Eur Radiol (2004) 14:341–349
DOI 10.1007/s00330-003-2084-4

EXPERIMENTAL

Hoen-Oh Shin
Christian V. Falck
Michael Galanski

Low-contrast detectability in volume rendering: a phantom study on multidector-row spiral CT data

Received: 24 April 2003
Revised: 10 July 2003
Accepted: 1 September 2003
Published online: 11 October 2003

H.-O. Shin (✉) · C. V. Falck · M. Galanski
Department of Diagnostic Radiology,
Medical School Hannover,
Carl-Neuberg-Strasse 1, 30625 Hannover,
Germany
e-mail: shin.hoen-oh@mh-hannover.de
Tel.: +49-511-5322664
Fax: +49-511-5323797

Abstract To cope with the increasing amount of CT data, there is growing interest in direct volume-rendering techniques (VRT) as a diagnostic tool. The aim of this phantom study was to analyze the low-contrast detectability (LCD) of VRT compared with multi-planar reformations (MPR). Soft tissue lesions were simulated by spheres of different diameters (3–8 mm). The average lesion density was 15 HU compared with a background density of 35 HU. Two different CT protocols with 40 and 150 mAs were performed on a multi-detector row CT. The scanning parameters were as following: 140 kV; 2×0.5-mm slice collimation; pitch 2 (table movement per rotation/single slice collimation), and reconstruction with 0.5-mm slice thickness at 0.5-mm interval. A B30 kernel was used for reconstruction. The VRT was performed by mapping Hounsfield values to gray levels equal to a CT window (center: 60 HU; window: 370 HU). A linear ramp was applied for the opacity transfer function varying the maximum opacity between 0.1 and 1.0. A statistical method based on the Rose model was used to calculate the detection threshold depending on lesion size and image noise. Additionally, clinical data of 2 patients with three liver lesions of different sizes and density were evaluated. In VRT, LCD was most dependent on object size. Regarding lesions larger than 5 mm, VRT is significantly superior to MPR ($p<0.05$) for all opacity settings. In lesions sized 3–5 mm a maximum opacity level approximately 40–50% showed a near equivalent detectability in VRT and MPR. For higher opacity levels VRT was superior to MPR. Only for 3-mm lesions MPR performed slightly better in low-contrast detectability ($p<0.05$). Compared with MPR, VRT shows similar performance in LCD. Due to noise suppression effects, it is suited for visualization of data with high noise content.

Keywords Volume rendering · Three-dimensional imaging · Multi-detector row CT · Low-contrast detectability

Introduction

Continuous development in CT technology leads to an increased quantity and quality of image data. With the present multidetector row scanners nearly isotropic data sets can be generated in daily work and with the advent of 16 channel multidetector row scanners isotropic scans can be performed routinely allowing high quality three-dimensional visualization.

A film-based reading cannot cope with this large amount of data [1, 2]. The present standard for soft copy reading is multi-planar reformation (MPR) in addition to cine viewing.

Three-dimensional techniques, such as surface-shaded display (SSD) and maximum intensity projections (MIP), are widespread tools for 3D presentation of high contrast applications such as bone examinations or CT angiography; however, they are not generally used for

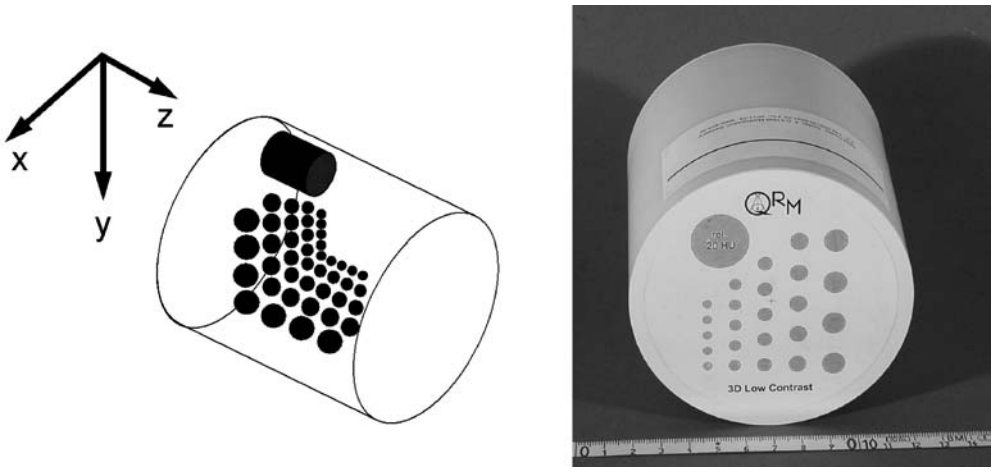

Fig. 1 Low-contrast phantom composed of spheres in different sizes (7×8 mm, 9×3–6 mm) and orientation (longitudinal/transversal). The spheres (15 HU) are embedded in "solid fluid" (35 HU)

primary diagnosis as three-dimensional visualization of these examinations demands a time-consuming manual or semi-automatic segmentation.

During the past years volume rendering (VRT) has become another useful method for 3D visualization and presentation. Due to the increasing computer power and the development of dedicated acceleration hardware it can now be realized as a real-time system with standard personal computers at reasonable costs [3, 4, 5, 6, 7].

Volume-rendering techniques may offer 3D information on anatomic structures without preprocessing CT data; thus, increasing the interest on this technique as a diagnostic tool. Several attempts have already been made to use VRT as a means of diagnosis in which VRT proved helpful in finding an accurate diagnosis in a number of questions. [8, 9, 10, 11, 12].

In many CT examinations, such as abdominal imaging (e.g., detection of focal liver lesions), a good performance in low contrast discrimination is essential.

The aim of this phantom study was to analyze the low-contrast detectability of VRT compared with multiplanar reformation (MPR). The results of the phantom study were compared with clinical examples of low-contrast lesions of the liver.

Materials and methods

Data acquisition: phantom

For evaluation of low-contrast resolution a 3D phantom (QRM GmbH, Moehrendorf, Germany) was used. Soft tissue lesions were simulated by spheres of different diameters ranging from 3 to 8 mm. The spheres were placed along all three directions. The average lesion density was 15 HU compared with 35 HU at the background; thus, the resulting contrast between spheres and surrounding "solid fluid" medium was −20 HU (Fig. 1). As low-contrast resolution is significantly influenced by noise, two different CT protocols with 40 and 150 mAs were performed on a multi-detector row CT (Siemens VolumeZoom, Forchheim, Germany); thus, the performance of VRT could be evaluated for different noise levels. The remaining scan parameters were as follows: 140 kV; 2×0.5-mm slice collimation; pitch 2 (table movement per rotation/single slice collimation); and reconstruction with 0.5-mm slice thickness at 0.5-mm interval. A standard kernel for abdominal imaging (B30) was used for the reconstruction of the axial source images. Using a field of view of 256-mm isotropic data sets with voxel lengths of 0.5 mm were realized. Two mAs settings were used to evaluate the performance of VRT for different noise levels. Following reconstruction, the data sets were transferred to the VRT workstation using a DICOM network.

Data acquisition: patients

To clinically evaluate the results of the phantom study, three liver lesions of different sizes and densities were retrospectively chosen from multidector-row spiral CT scans of 2 patients (Table 1). All CT scans were performed on a GE Lightspeed QX/i (General Electric, Milwaukee, Wis.) 4-channel multi-detector row scanner: 140 kV; 240 mAs; slice collimation 4×2.5 mm; pitch 6 (table movement per rotation/single-slice collimation), and reconstruction with 3-mm slice thickness at 2-mm interval. For further processing all data sets were transferred to the VRT workstation using the DICOM protocol.

Volume rendering

Volume visualization was performed on a standard PC (Dual Intel Pentium III 1 GHz, 2 GB RAM, GeForce 3 64 MB graphics, Windows 2000) which was equipped with a VolumePro1000 PCI board (TerraRecon, San Mateo, Calif.) for real-time volume rendering. Following data conversion, a Tcl/Tk script utilizing the image processing library of the Visualization Toolkit 4.0 (http://www.public.kitware.com/VTK/) with integrated functionality for the VolumePro VP 1000, was used to visualize all data sets. Depending on the density value of each voxel, a certain color and opacity was assigned for volume rendering. The transfer functions were defined as follows: the color transfer function was set to a standard CT abdomen window (center: 60 HU; window: 370 HU). The opacity transfer functions were defined as linear ramps at the same interval as the color transfer function. The ramp started at 0% opacity at the lower end while the maximum opacity was varied between 10 and 100% at the upper end of the window. A step size of 10% was used (Fig. 2). No gradient-transfer function was applied as it modulates the opacity. The volume was properly adjusted to get a standard, axial viewing direction. By cropping the

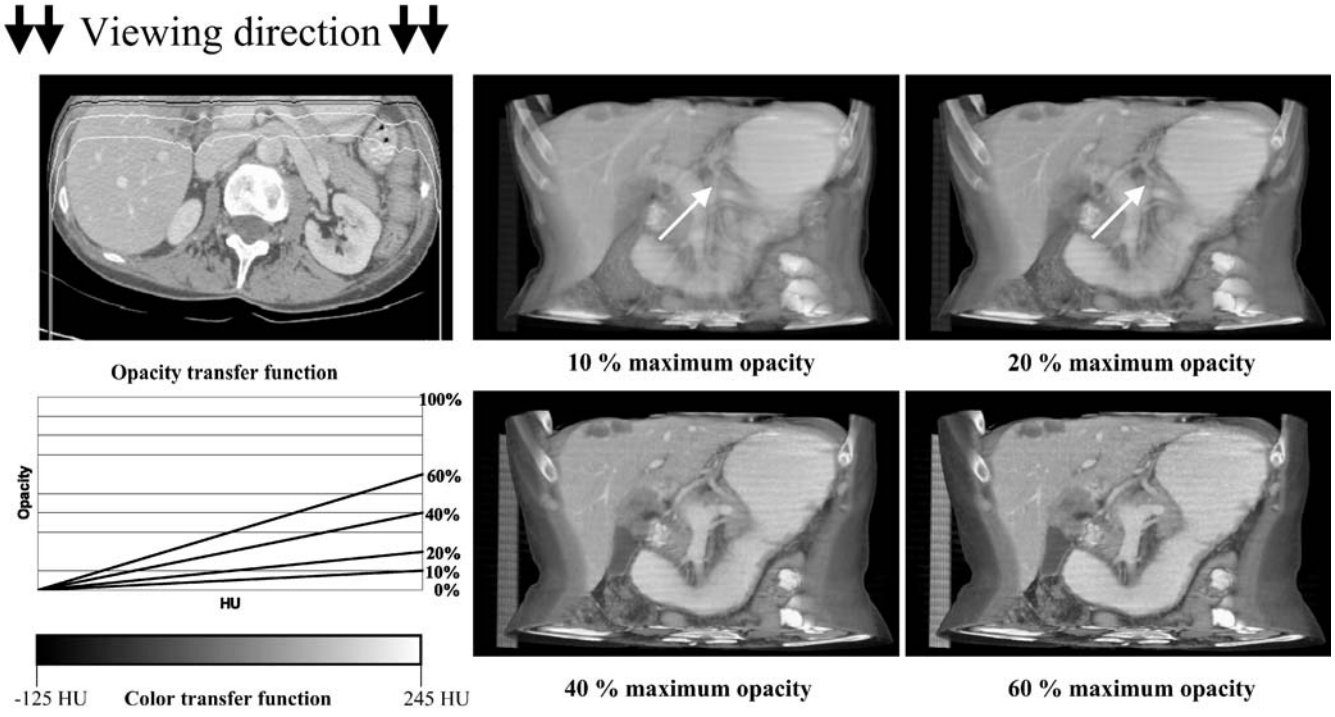

Fig. 2 Parameter settings for volume rendering: an abdominal window (center: 60 HU; width: 370 HU) was applied for the color transfer function. A linear ramp with varying maximum opacity settings was used for the opacity transfer function. There is an exponential decrease in "penetration length" with increasing maximum opacity values (*upper left image:* white: 0.1/0.2, gray: 0.4; black: 0.6). The lower the maximum opacity, the higher the penetration length (3D appreciation) and noise suppression. On the other hand, low maximum opacity values result in decrease of contrast. Note that the superior mesenteric artery (*arrows*) is only visible with maximum opacity settings of 0.1 and 0.2. With 0.4 and 0.6 the penetration length is not sufficient for visibility

Table 1 Evaluated patient data. *HU* Hounsfield units, *ROI* region of interest, *SD* standard deviation

Patient A	64-year-old woman
History	Carcinoid tumor of the small intestine with hepatic metastasis
CT	Multiple hypo- and hyperdense lesions
Lesion 1 (arterial phase)	ROI lesion: 118 HU (SD±10 HU) ROI parenchyma: 90 HU (SD±11 HU) ROI diameter: 14 mm
Lesion 2 (arterial phase)	ROI lesion: 23 HU (SD±9 HU) ROI parenchyma: 92 HU (SD±12 HU) ROI diameter: 4 mm
Patient B	67-year-old man
History	Hepatocellular carcinoma, hepatic cirrhosis
CT	Cirrhotic liver; hypodense lesion in segment V
Lesion I (portal venous phase)	ROI Lesion: 90 HU (SD±28 HU) ROI parenchyma: 105 HU (SD±27 HU) ROI diameter: 20 mm

data volume applying a moving, orthogonal cutting plane along the z-axis, different subvolumes were generated for volume rendering. Cropping was performed at regular intervals equal to the size of the reconstruction interval (0.5 mm). Each of the resulting images of the volume rendered subvolumes were saved for further processing in a standard image format (TIFF).

Image analysis

The Hounsfield values of the lesions in the phantom were assessed by placing large circular regions of interest (ROI) within the calibration cylinder and in the background. The measured object contrast was 19.4 HU for the 150 mAs scan and 17.7 HU for the 40 mAs scan. As no Hounsfield values could be derived from volume-rendered images, grey level differences were calculated to assess the performance of VRT in comparison with MPR. For MPR measurements, axial images of 0.5 mm thickness were applied. Prior to measurements of gray levels on MPR images an abdominal window (center: 60 HU; width: 370 HU) was applied. All measurements were performed on the same personal computer used for volume rendering. For calculation of gray-level differences ImageJ 1.24 (http://www.rsb.info.nih.gov/ij/) was utilized

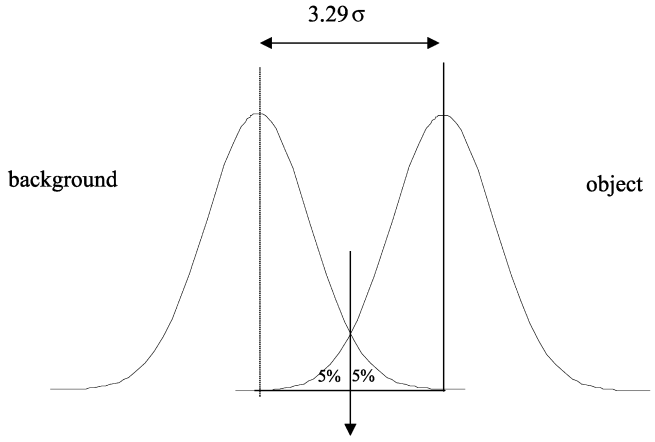

Fig. 3 Distribution of the mean CT value of the background and the object to be detected (assuming normal distribution). If the true CT value of the object is equal to 3.29σ standard deviation of the means, it can be detected at a 95% confidence interval

for both, volume rendered and reformatted images. The ROIs were placed in all visible lesions and in the background. The size of ROIs were chosen to nearly completely fill in the lesions. The smallest ROIs were used for 3-mm lesions (5×5 pixels). For each lesion size 4 ROIs were analyzed. The ROI positions and sizes were fixed for all transfer functions. The mean gray-level value and the standard deviation (SD) were measured for each ROI in every volume-rendered image. Contrast was calculated as the difference in mean brightness between the ROI and the background in the same image. Signal-to-noise ratio (SNR) was defined as the ratio of contrast to SD of the background.

Low-contrast detectability

Low-contrast detectability was measured using a statistical, reader-independent method. Similar methods have been previously published [13, 14] and are used by GE Medical Systems to measure the LCD published in their LightSpeedPlus technical data sheet.

During the 1940s Rose proposed a formula to calculate a minimum SNR for the detection of small circular objects in the presence of poisson-distributed image noise [15]; however, due to the fact that CT noise has a unique characteristic and is not regularly distributed, the measurement of the pixel noise itself is only of limited interest in determining the LCD. Instead, the standard deviation of the means of several ROIs placed on the image is more useful to determine the LCD. Basically, the dependencies between object size and noise characteristics are taken into account by performing noise analysis for different object sizes. Assuming a normal distribution of the means, a prediction can be made about the minimum contrast necessary for the detection of an object of the same size (area) as the ROI (Fig. 3). The measurement can be repeated with different ROI sizes in order to obtain a contrast discrimination function (CDF). In this study, we made use of this statistical method to analyze the influence of VRT on LCD. For VRT, a transfer function was applied to the data set; thus, noise had to be analyzed on the basis of gray values instead of Hounsfield units. Nevertheless, this method is applicable, as it does not require a regular noise distribution.

In practice, an array of square ROIs was placed on the center of a uniform part of the phantom, the mean gray values were measured, and the standard error of the means was calculated (Fig. 4). This measurement was repeated with ascending ROI sizes from 1^2 to 15^2 pixels for all opacity settings. Beween 100 to 5625 separate calculations were performed for each parameter setting. The distribution of the means was checked for normal distribution (Kolmogorov-Smirnoff test) and then multiplied by the factor 3.29 (for a 95% confidence interval) to obtain the minimum contrast necessary for detection. Mathematica 4.0 with Digital Image Processing Add-On (Wolfram Research, Champaign, Ill.) was applied for this computation.

For comparison of volume-rendered images to MPR using patient data, only contrast-to-noise ratios (CNR) were calculated as the statistical model was not applicable. This was due to the lack of a homogenous background on patient data which is necessary for computing the size-dependent noise frequency spectrum.

Results

Phantom study

For both phantom scans, the resulting gray-level differences between lesion and background for different opacity settings and MPR are summarized in Table 2. With increasing maximum opacity settings the image contrast

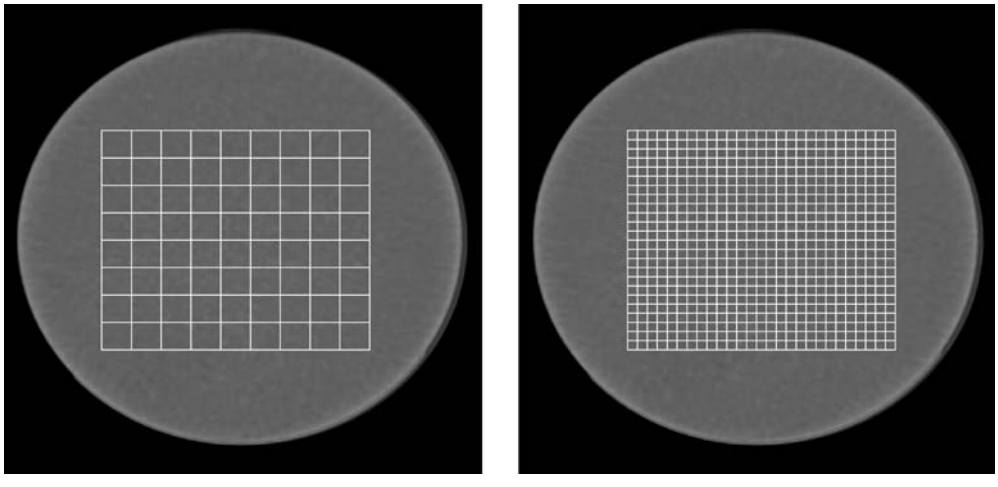

Fig. 4 Analysis of image noise: an array of square regions of interest (ROIs) is placed at the center of the image. Mean intensity is measured for each ROI. The standard error in the means is calculated and used to make a prediction about the minimal contrast necessary for detection of a lesion of the same size as the square ROIs. Analysis is repeated for different ROI sizes to obtain a function of detectability depending on lesion size

Table 2 Image contrast (mean gray-level difference) of the 40- and 150-mAs scan depending on applied transfer function and lesion size. *MPR* multi-planar reformations

Maximum opacity (%)	Lesion diameter (mm)															
	3 mm		4 mm		5 mm			6 mm			8 mm					
	40 mAs	150 mAs			40 mAs		150 mAs		40 mAs		150 mAs		40 mAs		150 mAs	
10	–	–	1.5	(±0.5)	0.4	(±0.3)	1.5	(±0.6)	0.9	(±0.2)	1.5	(±0.3)	1.7	(±0.5)	2.0	(±0.5)	3.4	(±0.4)	3.2	(±0.7)
20	–	–	2.3	(±0.3)	1.5	(±0.2)	2.8	(±0.6)	2.7	(±0.3)	3.2	(±0.6)	3.4	(±0.4)	3.8	(±0.4)	5.6	(±0.4)	5.4	(±0.5)
30	–	–	3.3	(±0.4)	2.6	(±0.4)	4.1	(±0.6)	4.2	(±0.4)	4.6	(±0.8)	4.8	(±0.4)	5.4	(±0.4)	7.5	(±0.5)	7.1	(±0.4)
40	–	–	3.9	(±0.5)	3.6	(±0.7)	5.1	(±0.7)	5.5	(±0.5)	5.7	(±0.9)	6.0	(±0.5)	6.6	(±0.4)	9.0	(±0.5)	8.5	(±0.3)
50	–	–	4.7	(±0.6)	4.4	(±0.8)	6.3	(±0.8)	6.6	(±0.6)	6.8	(±1.0)	7.1	(±0.6)	7.8	(±0.4)	10.1	(±0.5)	9.6	(±0.3)
60	–	–	5.4	(±0.7)	5.3	(±0.9)	7.2	(±0.8)	7.6	(±0.7)	7.7	(±1.0)	8.0	(±0.7)	8.8	(±0.4)	11.0	(±0.5)	10.5	(±0.3)
70	–	–	5.9	(±0.6)	5.9	(±0.9)	7.9	(±0.9)	8.3	(±0.8)	8.2	(±1.1)	8.8	(±0.8)	9.5	(±0.5)	11.8	(±0.6)	11.2	(±0.3)
80	–	–	6.5	(±0.5)	6.7	(±1.0)	8.6	(±0.8)	9.2	(±1.0)	8.9	(±1.0)	9.6	(±0.9)	10.1	(±0.5)	12.4	(±0.8)	11.7	(±0.4)
90	–	–	7.2	(±0.6)	7.2	(±0.9)	9.3	(±1.0)	9.7	(±1.0)	9.4	(±1.2)	10.2	(±1.1)	10.6	(±0.6)	12.9	(±0.8)	12.2	(±0.2)
100	–	–	7.6	(±0.5)	7.7	(±0.8)	9.8	(±1.0)	10.2	(±1.1)	9.8	(±1.3)	10.7	(±1.2)	11.0	(±0.6)	13.3	(±0.9)	12.5	(±0.2)
MPR	–	–	13.8	(±1.9)	12.2	(±0.2)	16.2	(±0.9)	16.6	(±0.9)	14.7	(±0.8)	14.5	(±1.4)	13.9	(±0.7)	15.0	(±1.5)	14.0	(±0.4)

No measurements could be attained in the 40-mAs scan for 3-mm lesions (dashes: lesions could not be clearly identified to place ROIs). Contrast is given as mean gray-level difference between lesion and background. Standard deviation is given in parentheses. With increasing maximum opacity settings the image contrast also increases but never reaches the image contrast in MPR for all evaluated lesion sizes.

Fig. 5 Visibility of volume-rendered images against multi-planar reformations (MPR) for the **a** 40-mAs and **b** 150-mAs scan (visibility of MPR is 100%). For lesions ≥5 mm a maximum opacity setting of 0.4 or larger allow a better visibility than MPR. For smaller lesions (3–4 mm) a maximum opacity setting of 0.5 or higher is required for the same visibility

Table 3 Image noise depending on applied scan dose (40 vs 150 mAs). Absolute SD is given in parentheses. Noise contribution increases with higher maximum opacity values and is highest on MPR images for both the 40- and the 150-mAs scan

Maximum opacity (%)	Scan protocol			
	40 mAs		150 mAs	
10	1.275	(±0.03)	1.24	(±0.017)
20	1.658	(±0.05)	1.31	(±0.056)
30	2.025	(±0.07)	1.50	(±0.072)
40	2.321	(±0.09)	1.60	(±0.081)
50	2.616	(±0.11)	1.76	(±0.084)
60	2.858	(±0.13)	1.86	(±0.088)
70	3.058	(±0.15)	1.90	(±0.089)
80	3.34	(±0.18)	2.00	(±0.093)
90	3.521	(±0.20)	2.08	(±0.100)
100	3.732	(±0.22)	2.16	(±0.105)
MPR	7.261	(±0.51)	3.88	(±0.245)

also increases but never reaches the image contrast in MPR for all evaluated lesion sizes. But concurrently, the magnitude of noise also increases with higher maximum opacity values and is highest on MPR images (Table 3). As expected, higher gray-level differences were necessary for visibility with decreasing lesion size; however,

Table 4 Calculated minium gray-level difference necessary for detection. The detection thresholds at a 95% CI were calculated utilizing a statistical analysis of image noise in the VRT/MPR images. The necessary image contrast for a particular lesion size decreases with lower opacity values. This is due to the noise suppressing effect of volume-rendering techniques (VRT) and partially compensates the observed loss in image contrast

Maximum opacity (%)	Lesion diameter									
	3 mm		4 mm		5 mm		6 mm		8 mm	
	40 mAs	150 mAs	40 mAs	150 mAs	40 mAs	150 mAs	40 mAs	150 mAs	40 mAs	150 mAs
10	3.9	2.5	3.4	2.2	3.1	2.2	3.1	2.1	2.6	1.9
20	4.7	2.9	4.2	2.5	3.6	2.4	3.4	2.2	2.8	2.0
30	5.6	3.4	4.8	2.9	4.1	2.6	3.8	2.4	3.1	2.1
40	6.3	3.7	5.4	3.2	4.5	2.8	4.1	2.5	3.3	2.2
50	7.0	4.0	6.0	3.4	4.9	3.0	4.5	2.6	3.5	2.3
60	7.7	4.2	6.6	3.6	5.4	3.1	4.8	2.7	3.7	2.4
70	8.3	4.5	7.1	3.8	5.8	3.3	5.1	2.8	3.9	2.4
80	9.2	4.8	7.7	4.1	6.3	3.5	5.6	2.9	4.3	2.5
90	9.6	5.0	8.1	4.2	6.6	3.6	5.7	3.0	4.4	2.5
100	10.2	5.3	8.6	4.5	7.1	3.8	6.1	3.2	4.7	2.6
MPR	20.1	10.1	16.5	8.7	14.0	7.1	11.6	6.1	9.3	4.7

Table 5 Variation of visibility depending on applied transfer function and lesion size

Maximum opacity (%)	Lesion diameter									
	3 mm		4 mm		5 mm		6 mm		8 mm	
	40 mAs	150 mAs	40 mAs	150 mAs	40 mAs	150 mAs	40 mAs	150 mAs	40 mAs	150 mAs
10	–	0.6^{-}	0.1^{-}	0.7^{-}	0.3^{-}	0.7^{-}	0.5^{-}	0.9^{-}	**1.3**	1.7^{-}
20	–	0.8^{-}	0.4^{-}	1.1^{-}	0.8^{-}	1.4^{-}	1.0^{-}	1.7^{-}	**2.0**$^{+}$	**2.7**
30	–	1.0^{-}	0.5^{-}	1.4^{-}	1.0^{-}	**1.8**	**1.3**	**2.3**	**2.5**$^{+}$	**3.3**
40	–	1.1^{-}	**0.7**	**1.6**	**1.2**	**2.0**	**1.4**	**2.7**$^{+}$	**2.7**$^{+}$	**3.9**$^{+}$
50	–	**1.2**	**0.7**	**1.9**	**1.3**	**2.3**	**1.6**$^{+}$	**3.0**$^{+}$	**2.9**$^{+}$	**4.2**$^{+}$
60	–	**1.3**	**0.8**	**2.0**	**1.4**$^{+}$	**2.5**	**1.7**$^{+}$	**3.3**$^{+}$	**3.0**$^{+}$	**4.5**$^{+}$
70	–	**1.3**	**0.8**	**2.1**	**1.4**$^{+}$	**2.5**	**1.7**$^{+}$	**3.4**$^{+}$	**3.0**$^{+}$	**4.7**$^{+}$
80	–	**1.3**	**0.9**	**2.1**$^{+}$	**1.4**$^{+}$	**2.6**$^{+}$	**1.7**$^{+}$	**3.4**$^{+}$	**2.9**$^{+}$	**4.7**$^{+}$
90	–	**1.4**	**0.9**	**2.2**$^{+}$	**1.5**$^{+}$	**2.6**$^{+}$	**1.8**$^{+}$	**3.5**$^{+}$	**2.9**$^{+}$	**4.9**$^{+}$
100	–	**1.4**	**0.9** $^{+}$	**2.2**$^{+}$	**1.4**$^{+}$	**2.6**$^{+}$	**1.8**$^{+}$	**3.4**$^{+}$	**2.9**$^{+}$	**4.8**$^{+}$
MPR	–	1.4	0.7	1.9	1.2	2.1	1.3	2.3	1.6	3.0

The numbers are the quotient of measured contrast and calculated minimum gray-level difference necessary for detection. A relative visibility of 1 represents the detection threshold. Maximum opacity settings with equal or better performance than MPR are boldface. Note that with increasing size, lower maximum opacity values can be used without losing visibility against MPR. Very small lesions (≤3 mm) do not allow low opacity settings while in lesions ≥8 mm VRT even equals MPR's low-contrast detectability at a 20% opacity level. +/– indicate significant (p<0.05) difference to MPR.+ indicates superior, – inferior visibility compared with MPR. No measurements could be attained in the 40-mAs scan for 3-mm lesions (dashes), as the lesions could not be clearly identified

interestingly, MPR needed much higher gray-level differences for detection than VRT for all lesion sizes (Table 4).

In Table 5 the quotient was formed of measured contrast and calculated minimum gray-level difference: 1 represents the detection threshold, values lower than 1 mean not visible. In comparison with MPR a maximum opacity level around 40% showed a near equivalent detectability in VRT for lesion sizes of 5 mm and is only slightly inferior for smaller lesions. For larger lesions this setting is significantly superior to MPR (Fig. 5); thus, a linear ramp with a maximum opacity value of 0.4 appeared to be a good start for viewing. This is true for both, the 150- and the 40-mAs scans, indicating that optimal presets for VRT are mostly independent of the noise magnitude. In Fig. 6 MPR and three different maximum opacity settings are put side to side. At first glance MPR looks superior to VRT, but this is due to the different image characteristics of VRT. At a closer look the 5 mm and larger lesions are equally/better delineated in the VR images for maximum opacity values of 0.4 and 0.6, especially in the noisy 40-mAs data. The 4-mm spheres show an equivalent performance to MPR for maximum opacity of 0.6. The visibility of 3-mm lesions

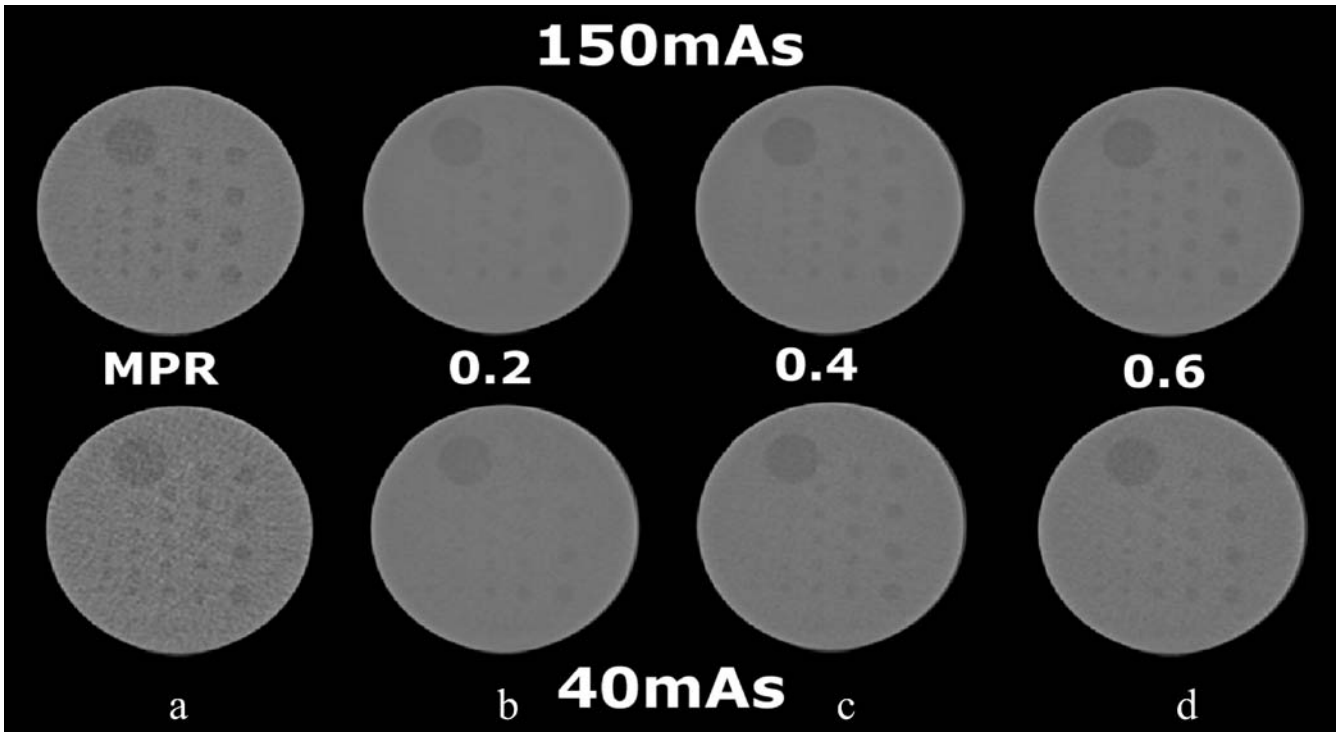

Fig. 6 The MPR and three different maximum opacity settings, side to side. At first glance MPR looks superior to VRT, but this is due to the different image characteristics of VRT. At a closer look the 5 mm and larger lesions are equally/better delineated in the VR images for maximum opacity values of 0.4 and 0.6, especially in the noisy 40-mAs data

in VRT is inferior to MPR for the depicted maximum opacity settings.

Clinical cases

As explained in "Materials and methods" the statistical model was not applicable to clinical data. For comparison of volume rendered images to MPR using patient data, contrast-to-noise ratios (CNR) were calculated. Although CNR is not as precise as the statistical model, both the hyper- (Pat A I) and the hypodense lesion (Pat B I) showed a higher CNR on VR images than on MPR for all opacity settings. Only the very small third lesion (Pat A II) presented a lower CNR on VR images than MPR (Table 6). These results confirm the findings of the phantom study. Except for very small lesions, VR images show a higher performance regarding visibility of low-contrast lesions than MPR. Figure 7a illustrates MPR and VR images of lesion I from patient B. Multiple lesions of patient A are presented in Fig. 7b. As VRT contains information from more than one plane, the extent of lesions is better assessed than in MPR and the appreciation of the spatial relationship between lesions and intraparenchymal vessels is also improved.

Table 6 Contrast-to-noise (CNR) ratio of the lesions in Table 1 for different maximum opacity settings and MPR. The CNRs are given in percentage relative to MPR. For technical reasons the statistical method used for the evaluation of the phantom could not be used with patient data. Image quality is therefore assesed by calculating the CNR

Maximum opacity (%)	Patient A I (%)	Patient B I (%)	Patient A II (%)
10	100.72	251.95	42.88
20	136.54	209.17	61.51
30	145.49	179.38	70.52
40	137.86	165.92	75.45
50	136.51	151.44	78.47
60	127.90	143.36	80.36
70	127.58	135.18	83.67
80	122.24	127.86	88.63
90	115.20	122.13	91.42
100	108.01	116.63	90.32
MPR	100.00	100.00	100.00

Discussion

The aim of this study was to analyze the low-contrast performance of volume rendering and to find appropriate settings for the opacity transfer function. Although larger databases have to be evaluated to find optimal settings of the transfer functions, this study shows the principle suitability of volume rendering as a diagnostic tool for low-contrast lesions. Although our selection of transfer functions might not be optimal, it showed comparable low-contrast resolution to MPR; thus, if better transfer func-

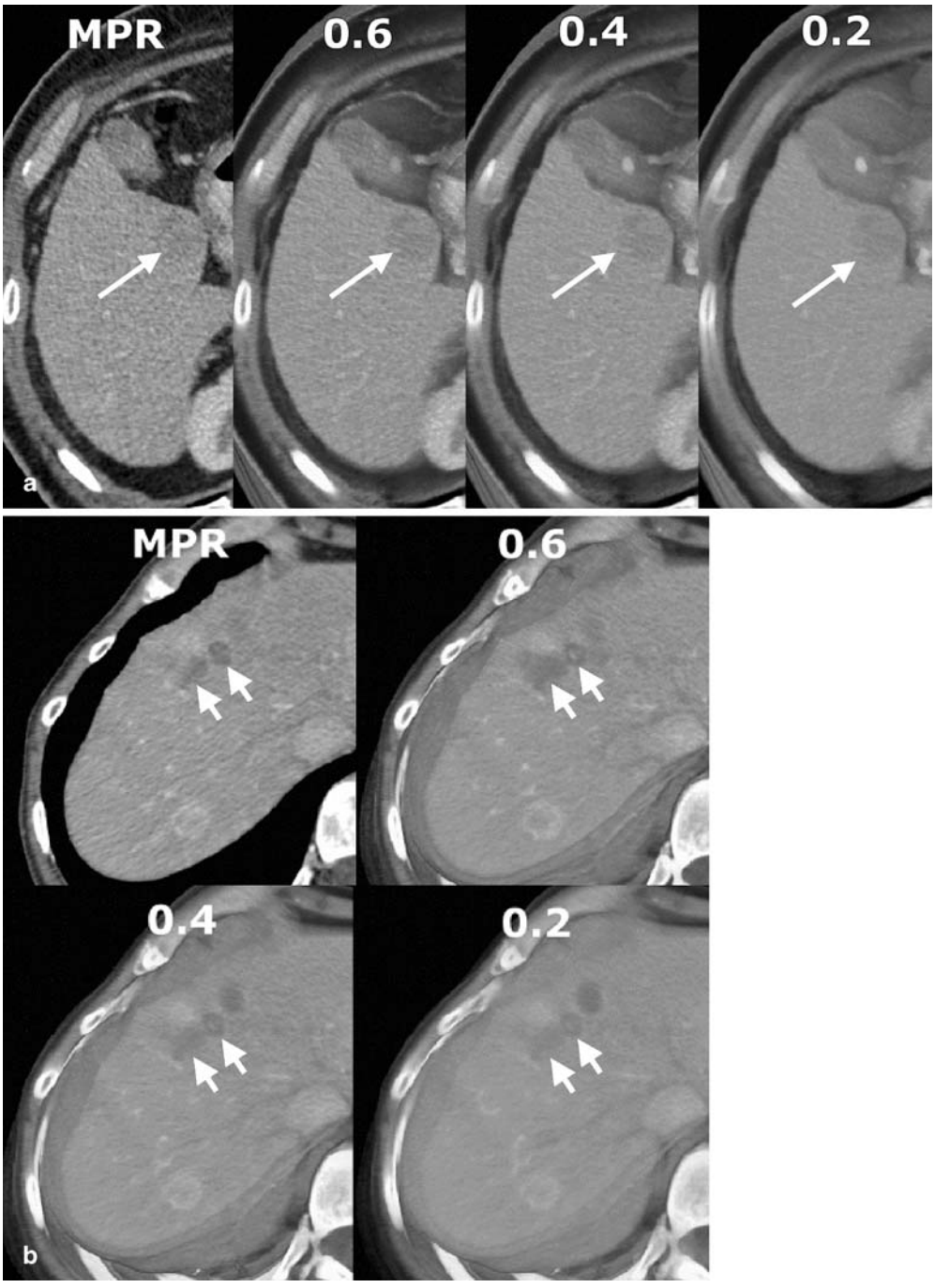

Fig. 7 a Patient B with hepatocellular carcinoma shows a solitary, low-density mass in the right lobe (segment V) of the liver (*arrows*). Because of its size and noise suppression in volume-rendering techniques (VRT), visibility is superior to MPR for all maximum opacity settings. **b** Patient A (dual-phase scan, data from arterial phase): multiple masses of varying size and density representing metastases from carcinoid tumor of the small intestine. In VRT, the extent of the lesions and the uptake of contrast agent are better appreciated (*arrows*). Also note the better delineation of hyperdense rim around some of the masses

tions exist, the performance of VRT will further improve. In VRT, low-contrast detectability is dependent on object size. For very small lesions (3 mm and smaller) MPR is still superior. This is due to a "smoothing" effect of the calculations in VRT resulting in noise suppressed but lesser visible images of very small objects. For larger objects, visibility in VRT is better than in MPR.

The specification of transfer functions is a difficult task [16, 17]. Although individual adaptation of parameters yields the best results, a fixed setting is preferable for clinical applications. Using standardized settings of transfer functions no time-consuming manipulation of parameters is required. In current practice the color transfer function, which determines the visible data range, is defined by mapping Hounsfield values to a linear ramp of increasing gray levels equal to a CT window for soft tissue visualization (window level: 60 HU; window width: 370 HU). This appears to be a good standard

setting as the CT window is already optimized for best visibility and contrast of the interesting anatomy and potential pathologies. Color proved to be of moderate help as with the exception of clearly separated tissue densities, such as, for example, air or bone, color coding of different tissues requires extensive adjustment of the color transfer function; thus, no colors were used in our study. A linear ramp was also applied for the opacity transfer function. Accordingly, higher density values were assigned to higher opacities, and brighter gray values.

Low maximum opacity values lead to a larger "penetration length" and thus to a better 3D appreciation. To take most advantage of VRT the maximum opacity should be set at the lower end still keeping the same contrast detectability as MPR; however, in rare cases, using a low maximum opacity value may lead to artifacts due to overlaying structures of similar densities along the viewing path possibly masking low-contrast lesions.

A great advantage of VRT is its ability of noise suppression allowing its application in scans with high noise content and utilization of "dose-wise" protocols for high-resolution imaging tolerating increased noise. For LCD, noise suppression in VRT mostly compensates the lower image contrast in comparison with MPR. The lower the maximum opacity setting, the higher the noise suppression; however, to take full advantage of VRT, interactive visualization, and manipulation of the data volume are essential. In combination with cutting tools for the selection of subvolumes, VRT provides an efficient way of reading large CT volumes. In current practice, we use a simple cutting plane or a sliding thin-slab VR technique for interactive viewing, preferably in the coronal direction; however, depending on anatomy, arbitrary viewing directions, including oblique ones, are necessary.

There are limitations of our study. Neither reconstruction kernels nor different reconstruction intervals were varied, and only one collimation set was applied; however, calculation errors due to partial-volume effects and undersampling (to be expected with larger collimations and reconstructions intervals) were minimized by using 2×0.5-mm collimation. Since LCD is directly dependent on image noise, and our results on low contrast discrimination are only based on measurements of two different noise levels, no universally applicable rules can be derived for low contrast visibility in general; however, the most favorable settings of the opacity transfer function calculated for both phantom scans are nearly identical suggesting only minor impact of the noise level to the optimal parameter settings. These assumptions were also confirmed for the examined clinical data. Further studies are warranted to evaluate whether VRT provides all necessary diagnostic information to make it eligible as a primary diagnostic tool (as a replacement or addition to planar viewing). Especially the performance of VRT in comparison to sliding thin-slab technique has to be assessed.

References

1. Rubin GD (2000) Data explosion: the challenge of multidetctor-row CT. Eur J Radiol 36:74–80
2. Roos JE, Desbiolles LM, Willmann JK, Weishaupt D, Marincek B, Hilfiker PR (2002) Multidetector-row helical CT: analysis of time management and workflow. Eur Radiol 12:680–685
3. Drebin RA, Carpenter L, Hanrahan P (1988) Volume rendering. Comput Graph 22:65–74
4. Ney DR, Drebin RA, Fishman EK, Magid D (1990) Volumetric rendering of computed tomography data: principles and techniques. IEEE Comput Graph Applicat 10:24–32
5. Calhoun PS, Kuszyk BS, Heath DG, Carley JC, Fishman EK (1999) Three-dimensional volume rendering of spiral CT data: theory and method. Radiographics 19:745–764
6. Fishman EK, Magid D, Ney DR, Chaney EL, Pizer SM, Rosenman JG et al. (1991) Three-dimensional imaging. Radiology 181:321–337
7. Pfistner H, Hardenbergh J, Knittel J, Lauer H, Seiler L (1999) The VolumePro real-time ray-casting system. Proc ACM SIGGRAPH:251–260
8. Kuszyk BS, Heath DG, Bliss DF, Fishman EK (1996) Skeletal 3-D CT: advantages of volume rendering over surface rendering. Skeletal Radiol 25:207–214
9. Pretorius ES, Fishman EK (1999) Volume rendered three-dimensional spiral CT: musculo-skeletal applications. Radiographics 19:1143–1160
10. Lawler LP, Fishman EK (2001) Multidetector row CT of thoracic disease with emphasis on 3D volume rendering and CT angiography. Radiographics 21:1257–1273
11. Urban BA, Ratner LE, Fishman EK (2001) Three-dimensional volume rendered CT. Angiography of the renal arteries and veins: normal anatomy, variants, and clinical applications. Radiographics 21:373–386
12. Ishifuro M, Horiguchi J, Nakashige A et al. (2002) Use of multidetector-row CT with volume renderings in right lobe living liver transplantation. Eur Radiol 12:2477–2483
13. ASTM (2001) Standard test method for measurement of computed tomography (CT) performance. ASTM E1695–1695
14. Chao EH, Toth TL, Bromberg NB, Williams EC, Fox SH, Carleton DA (2000) A statistical method of defining low-contrast detectability. Radiology 217:162
15. Hasegawa BH (1991) The Rose model. In: The physics of medical imaging, 2nd edn. Madison, Wisconsin, pp 219–231
16. Fang S, Biddlecom T, Tuceryan M (1998) Image-based transfer function design for data exploration in volume visualization. Proc of IEEE visualization: 319–326
17. König AH, Gröller EM. Mastering transfer function specification by using VolumePro Technology. http://www.cg.tuwien.ac.at/research/vis/vismed/ATFSpec/